


## Conformal invariance of weakly compressible two-dimensional turbulence

Leonardo Puggioni <sup>1</sup>, Alexei G. Kritsuk <sup>2</sup>, Stefano Musacchio,<sup>1</sup> and Guido Boffetta <sup>1</sup>

<sup>1</sup>*Dipartimento di Fisica and INFN, Università di Torino, via P. Giuria 1, 10125 Torino, Italy*

<sup>2</sup>*Center for Astrophysics and Space Sciences, University of California San Diego, 9500 Gilman Drive, La Jolla, California 92093-0424, USA*



(Received 11 June 2020; accepted 22 July 2020; published 10 August 2020)

We study conformal invariance of vorticity clusters in weakly compressible two-dimensional turbulence at low Mach numbers. On the basis of very high resolution direct numerical simulation we demonstrate the scaling invariance of the inverse cascade with scaling close to Kolmogorov prediction. In this range of scales, the statistics of zero-vorticity isolines are found to be compatible with those of critical percolation, thus generalizing the results obtained in incompressible Navier-Stokes turbulence.

DOI: [10.1103/PhysRevE.102.023107](https://doi.org/10.1103/PhysRevE.102.023107)

### I. INTRODUCTION

The inverse energy cascade is a key feature of two-dimensional (2D) incompressible turbulence predicted by Kraichnan many years ago [1]. As a consequence of the existence of two inviscid quadratic invariants of the 2D incompressible Navier-Stokes equations, the enstrophy is transferred to small scales producing the direct cascade, while energy moves to large scales generating the inverse cascade. The inverse cascade in 2D incompressible turbulence has been observed in numerical simulations [2–6] and laboratory experiments [7–9], and its scaling properties have been established, including the almost Gaussian statistics of velocity fluctuations and the absence of intermittency [5].

More recently, scaling invariance of the inverse cascade has been promoted to conformal invariance for some specific features of the turbulent field. In particular, by using the technique of stochastic-Löwner evolution (SLE), it has been shown that clusters of vorticity are statistically equivalent to those of critical percolation, one of the simplest universality classes in critical phenomena [10]. This result, which suggests an intriguing connection between (nonequilibrium) turbulent flows and statistical models at the critical point, has been extended to other 2D incompressible flows, including surface quasigeostrophic turbulence [11] and a class of active scalar turbulence [12]. Conformal invariance has also been investigated experimentally in Lagrangian reconstructed vorticity field of a turbulent surface flow [13] (2D section of a three-dimensional flow), where deviations from SLE predictions have been observed.

In this paper, we study the appearance of conformal invariance in the inverse cascade of weakly compressible 2D turbulence. Compressible 2D turbulence has applications in numerous geophysical, astrophysical, and industrial problems. Specifically, we consider a flow with an ideal-gas equation of state with the ratio of specific heats  $\gamma = c_v/c_p \simeq 1$ , which is relevant to astrophysical applications (where radiation provides for temperature equilibration) [14] and for soap films when fluid velocities are of the order of the elastic wave speed in the limit of large Reynolds numbers [15].

This paper is organized as follows. In Sec. II we introduce the physical model, its phenomenology, and the numerical simulation. In Sec. III we discuss the statistics of the inverse cascade, while Sec. IV is devoted to conformal analysis of isovorticity lines. Finally, Sec. V contains some conclusions.

### II. MODEL AND PHENOMENOLOGY OF 2D COMPRESSIBLE FLOWS

The dynamics of a compressible flow is given by the Euler equations, which impose the conservation of mass, momentum and total energy:

$$\partial_t \rho + \nabla \cdot (\rho \mathbf{u}) = 0, \quad (1)$$

$$\partial_t (\rho \mathbf{u}) + \nabla \cdot (\rho \mathbf{u} \mathbf{u} + p \mathbf{I}) = \mathbf{f}, \quad (2)$$

$$\partial_t \mathcal{E} + \nabla \cdot [(\mathcal{E} + p) \mathbf{u}] = \mathbf{f} \cdot \mathbf{u}, \quad (3)$$

where  $\rho$  is the density field,  $\mathbf{u}$  the velocity,  $p$  is the pressure,  $\mathbf{f}$  is the external forcing,  $\mathcal{E} = \rho(u^2/2 + e)$  is the total energy density (the sum of kinetic and potential energy density), and  $\mathbf{I}$  is the identity matrix. The system of equations (1)–(3) is closed by the equation of state for an idea gas  $p = (\gamma - 1)\rho e$ . In the absence of external forcing  $\mathbf{f} = 0$ , the system conserves the total energy  $E = \int \mathcal{E} d\mathbf{x}$ , which is given by the sum of the kinetic energy  $K = (1/2) \int \rho u^2 d\mathbf{x}$  and the potential energy  $U = \int \rho e d\mathbf{x}$ .

The average compressibility of the velocity field is quantified by the rms Mach number  $M = \sqrt{\langle u^2 \rangle}/c$ , where  $c$  is the speed of sound in the fluid. The velocity field can be decomposed into the solenoidal and irrotational components  $\mathbf{u} = \mathbf{u}_s + \mathbf{u}_i$ , where  $\nabla \cdot \mathbf{u}_s = 0$  and  $\nabla \times \mathbf{u}_i = 0$ .

In the case of a 2D flow, they can be expressed in terms of two scalar fields: The stream function  $\psi$  and the velocity potential  $\phi$ ,

$$\mathbf{u}_s = (\partial_y \psi, -\partial_x \psi), \quad (4)$$

$$\mathbf{u}_i = \nabla \phi. \quad (5)$$

The Laplacian of the velocity potential provides a local measure of the divergence of the velocity  $\nabla \cdot \mathbf{u} = \nabla^2 \phi$ , while the Laplacian of the stream functions defines the vorticity field  $\omega = \partial_x u_y - \partial_y u_x = -\nabla^2 \psi$ .

The phenomenology of a 2D compressible flow is strongly dependent on the Mach number. In the low-compressibility regime ( $M \ll 1$ ), the behavior is similar to that of the incompressible case. One observes the development of a double-cascade scenario in which the enstrophy  $\Omega = (1/2) \int \omega^2 \rho \, dx$  is preferentially transferred toward small scales (direct cascade), while the kinetic energy is transferred mostly to large scales (inverse cascade). In the absence of a large-scale dissipation mechanism (such as friction), the inverse cascade process causes the accumulation of energy at the largest scale (smaller wave number) of the flow. The phenomenon of “spectral condensation” of kinetic energy on the lowest accessible wave number [4] has been studied both in the 2D incompressible [16] and compressible flows [14,17]. It has also been observed in quasi-2D geometries, i.e., in the turbulent dynamics of thin layers [18,19].

The energy accumulation at large scales causes the growth in time of the Mach number, increasing the compressibility of the flow. A peculiar phenomenon of the compressible case is the formation of acoustic waves, i.e., pressure fluctuations which propagate within the fluid [20]. Acoustic waves of sufficiently large amplitude break to form a train of N-waves. Emerging shocks in turn speed up the attenuation of acoustic energy. Shocks also amplify small-scale vorticity by compression and produce new vorticity through shock-shock interactions, while strong shear generates new shocks and rarefaction waves [21,22]. At sufficiently large Mach numbers, the interaction between acoustic waves and vortices thus causes a transfer of energy toward small scales through wave breaking and the generation of shocks [14]. This provides a stabilizing mechanism for the energy of the condensate, which is fed by the inverse cascade process and is removed by the acoustic waves, allowing for the formation of a statistically steady state. This process resembles the so-called “flux loop” observed in 2D stratified flows [23]. While the dynamics of vortices and waves is strongly coupled at large scales, it has been found to be almost independent at small scales, where the cascade of wave energy follows the predictions of acoustic turbulence and is decoupled from the enstrophy cascade [14].

### Numerical simulation

The Euler equations (1)–(3) have been integrated by an implicit large eddy simulation (ILES) [24] in a square periodic domain of size  $L$  on a grid of  $8192 \times 8192$  points using an implementation of the piecewise parabolic method [25] with the *Enzo* code [26]. The reference length, time, and mass in the simulation are defined by choosing the box size  $L = 1$ , the speed of sound  $c = 1$ , and the mean density  $\rho_0 = 1$ . Starting from a zero initial velocity field, the system is forced by a solenoidal, random external forcing  $\mathbf{f}$  acting on an intermediate pumping scale  $L_f = 2\pi/k_f$  with  $k_f = 1024\pi$ . The time correlation of the forcing is of the order of the time step, i.e., much smaller to any physical timescale in the system. The rate of kinetic energy injection provided by the forcing is  $\varepsilon_f = 0.001$ . We remark that this value has to be

kept sufficiently small to avoid the production of shock waves at the injection scale, which would inhibit the inverse cascade of energy. The characteristic vortex turnover time at the scale  $L_f$  is  $\tau_f = \rho_0^{1/3} L_f^{2/3} \varepsilon_f^{-1/3} \simeq 0.52$ , which is more than  $10^4$  times larger than the forcing correlation time. The time integration has been performed up to time  $t = 30$  with a sampling of the velocity field and computation of the vorticity field every  $\Delta t = 0.05$ .

We remark that even if no explicit dissipative mechanism is prescribed in (1)–(3), the code introduces numerical dissipation which strongly affects scales smaller than  $16\Delta x$  ( $\Delta x = 1/8192$  is the spatial resolution).

### III. STATISTICS OF THE INVERSE CASCADE

The temporal evolution of the total energy  $E$ , the kinetic energy  $K$ , the enstrophy  $\Omega$ , and the Mach number  $M$  during the simulation is shown in Fig. 1. At the beginning of the simulation, the Mach number is very small and the dynamics of the system are dominated by its incompressible part. Therefore, we expect to observe the development of an inverse energy cascade propagating from the forcing scale  $L_f$  to larger scales  $r \gg L_f$  and a direct enstrophy cascade toward small scales  $r \ll L_f$ . This is confirmed by the linear growth of the total energy  $E \sim \varepsilon_{inv} t$  with a growth rate  $\varepsilon_{inv} \approx 0.92\varepsilon_f$ , which corresponds to the flux of energy in the inverse cascade. The total energy is dominated by the contribution of the kinetic energy  $K$ , while the potential energy  $U$  becomes visible only at late times  $t \gg 20$ .

In contrast to the energy, we find that after an initial growth, the enstrophy  $\Omega$  reaches an almost constant value (see Fig. 1). This happens because the direct enstrophy cascade transfers the enstrophy injected by the forcing to the small scales, where it is removed by numerical dissipation.

At late times, the inverse energy cascade will eventually produce an accumulation of the energy at the largest scale, giving rise to the formation of an intense vortex dipole (the

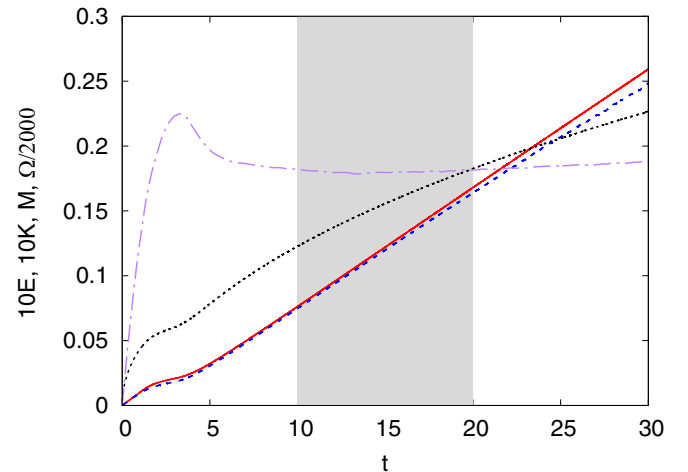


FIG. 1. Time evolution of the total energy  $E$  (red solid line), kinetic energy  $K$  (blue dashed line), enstrophy  $\Omega$  (purple dash-dotted line), and Mach number  $M$  (black dotted line). The values of  $E$  and  $K$  have been multiplied by a factor of 10 and  $\Omega$  by a factor of  $1/2000$  for plotting purposes.

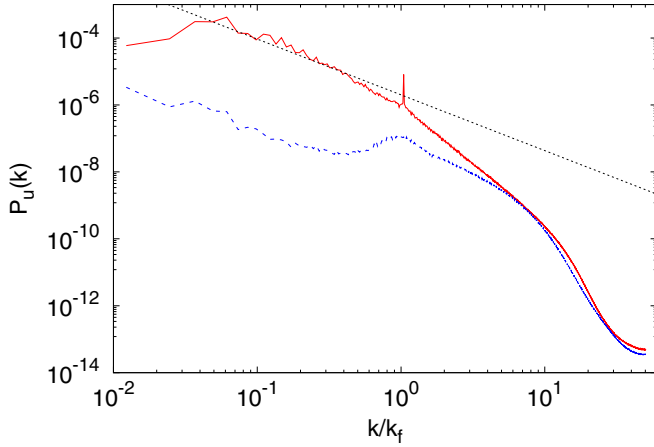


FIG. 2. Power spectra of the solenoidal component of the velocity  $P_s(k)$  (red solid line) and of the irrotational component  $P_i(k)$  (blue dashed line), at time  $t = 20$ . Black dotted line represents Kolmogorov scaling  $k^{-5/3}$ .

condensate). The formation of this vortical structure results in non-Gaussian statistics in the vorticity field and causes the breaking of scale invariance [27]. Considering that we are interested in the study of the conformal invariance of the vorticity field, it is crucial to verify that the field is at least scale-invariant. For this reason, in the following we will limit our analysis to the time range  $10 < t < 20$ , i.e., well before the beginning of the formation of the condensate. Moreover, in this time interval the value of  $\Omega$  is almost constant, which allows us to assume that the dynamics of the vorticity field are in a statistically steady state. In this time range, the Mach number varies from  $M \simeq 0.12$  at  $t = 10$  to  $M \simeq 0.18$  at  $t = 20$  (Fig. 1). The dynamics are therefore weakly compressible.

Furthermore, we will consider the scaling properties in the range of scales of the inverse cascade  $L_f \ll r \ll L$ , in which the conformal invariance has been detected for the case of 2D incompressible turbulence [10]. As shown in Fig. 2, in the range of wave numbers of the inverse cascade ( $0.04k_f < k < k_f$ ) the power spectrum of kinetic energy is dominated by the spectrum of the solenoidal component of the velocity field  $P_s(k) = \sum_{|q|=k} |\mathbf{u}_s(q)|^2$ , while the spectrum of the irrotational component  $P_i(k) = \sum_{|q|=k} |\mathbf{u}_i(q)|^2$  is much smaller (by more than a factor of 200 between  $0.04k_f < k < 0.4k_f$ ). The power spectrum of the solenoidal component  $P_s(k)$  displays an approximately Kolmogorov slope for wave numbers  $k < 0.6k_f$  with a steeper exponent close to  $-2$  close to the forcing scale [14,27]. At high wave numbers, the spectra of the irrotational and solenoidal components become comparable. With a more accurate numerical method and adaptively controlled numerical dissipation, two independent direct cascades can be resolved at  $k > k_f$ : The enstrophy cascade and the acoustic energy cascade. These are reflected in the scaling of power spectra,  $P_s(k) \sim k^{-3} \ln(k/k_f)$  and  $P_i(k) \sim k^{-2}$  [27]. While  $P_s(k)$  dominates at  $k \lesssim k_f$ ,  $P_i(k)$  inevitably becomes dominant at  $k \gg k_f$ .

Another indication of the scale invariance of the velocity field in the range of scales of the inverse energy cascade is provided by the third-order longitudinal structure function (SF)  $S_3(r) = \langle [\delta u_L(r)]^3 \rangle$  where  $\delta u_L(r) = [\mathbf{u}(\mathbf{x} + \mathbf{r}) - \mathbf{u}(\mathbf{x})] \cdot \mathbf{r}/r$

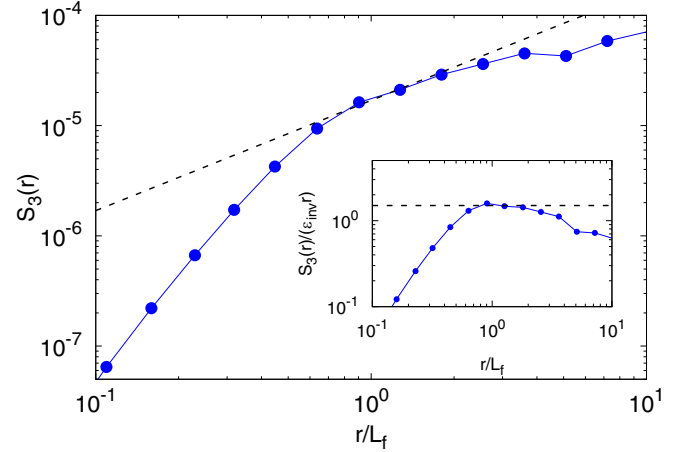


FIG. 3. Third-order longitudinal structure function  $S_3(r)$  (blue circles) average over times  $10 \leq t \leq 20$ . Black dashed line represents (6). Inset: Compensated structure function  $S_3(r)/(\varepsilon_{inv}r)$  (blue circles) and the predicted value  $3/2$  (black dashed line).

is the longitudinal velocity difference at scale  $r$ . In 2D incompressible turbulence, the constant energy flux in the inertial range gives an exact prediction for the third-order structure function which, in homogeneous and isotropic conditions, reads [28,29]

$$S_3(r) = \frac{3}{2} \varepsilon_{inv} r, \quad (6)$$

where  $\varepsilon_{inv}$  represent the inverse kinetic energy flux. The third-order SF, time averaged for  $10 < t < 20$  in our simulation, is shown in Fig. 3. It displays a linear scaling range at  $r > L_f$  with a coefficient  $\frac{3}{2} \varepsilon_{inv}$  (see inset of Fig. 3) in agreement with the assumption of a constant energy flux. Let us notice that, because of the lack of stationarity at large scales  $r \gg L_f$ , the scaling  $S_3(r) \sim r$  is observed only in a narrow range of scales.

#### IV. CONFORMAL INVARIANCE OF ISOVORTICITY LINES

The discovery of conformal invariance in 2D turbulence was first made for the zero-vorticity lines in incompressible Navier-Stokes equations [10] and then extended to other 2D turbulent systems characterized by different scaling laws [11,12]. These previous results suggest the possibility to also test conformal invariance in the inverse cascade of weakly compressible turbulence.

We have extracted the vorticity clusters (i.e., connected regions of positive or negative vorticity) and zero vorticity isolines (boundaries of vorticity clusters) from the different fields of the simulation. We have obtained an ensemble of  $N_c = 461\,399$  clusters. One example of these clusters is shown in Fig. 4 for an intermediate time in the simulation  $t = 20$ . Here we observe the presence of clusters of different sizes, each one enclosed by a complex, fractal boundary.

Figure 5 shows the probability distribution function (PDF)  $p(A)$  of cluster size  $A$ , defined as the number of connected sites which belong to the cluster. The PDF displays a power-law behavior in the range  $L_f^2 < A < 10L_f^2$ . The scaling exponent observed in Fig. 5 is in agreement with the theoretical value predicted in the case of critical percolation in 2D  $p(A) \sim A^{-96/91-1}$  [30]. The same value has been previously observed



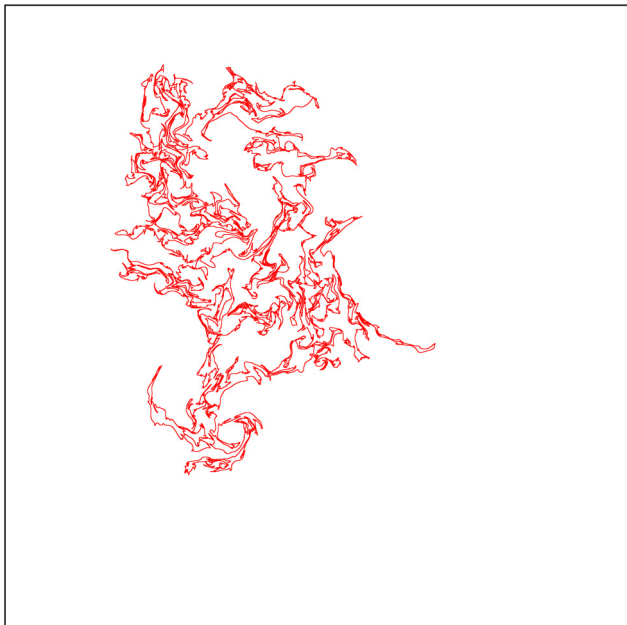
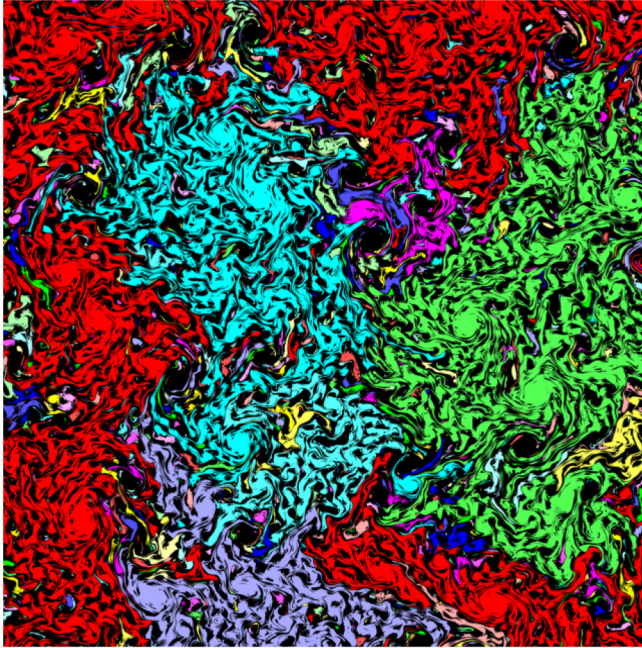


FIG. 4. Top: Vorticity cluster, defined as connected regions with the same sign of vorticity (here positive). Different colors are attributed to different clusters. Regions of negative vorticity are black. Bottom: Zero-vorticity isoline of the cyan cluster.

for the scaling exponent of the PDF of vorticity clusters' size in the case of incompressible 2D Navier-Stokes [10].

This result suggests that vorticity clusters produced by the inverse cascade in weakly compressible turbulence are statistically equivalent to clusters of critical percolation and therefore display the same properties of conformal invariance. In particular, the cluster boundaries in the continuous limit are expected to belong to the class of conformal curves called SLE curves [31,32]. In order to introduce briefly the basics of the SLE, let us consider a curve  $\gamma(s)$ , parameterized by the

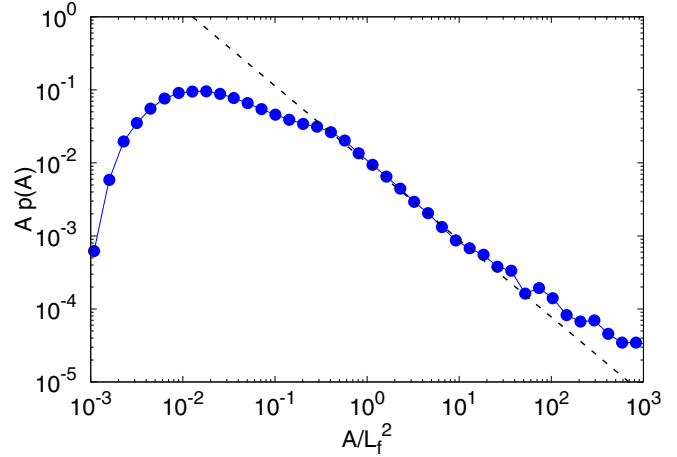


FIG. 5. Probability density function of cluster size  $A$  (blue circles). The black dashed line represents the scaling prediction by percolation theory  $Ap(A) \sim A^{-96/91}$ .

time  $s$ , starting from a point of the boundary of the half-plane  $H$ . At given time  $s$ , the curve  $\gamma(s)$  define a region  $K_s$  (the *hull*) formed by the points of the complex half-plane which cannot be reached from infinity without crossing the curve, plus the curve itself. The simply connected set  $H \setminus K_s$  can be mapped into  $H$  by an analytic function  $g_s(z)$  which satisfies the asymptotic behavior  $g_s(z) \sim z + 2s/z + O(z^{-2})$  at  $z \rightarrow \infty$ . The conformal map  $g_s(z)$  obeys the differential Löwner equation [33]:

$$\frac{dg_s}{ds} = \frac{2}{g_s(z) - \xi(s)}, \tag{7}$$

where  $\xi(s)$  is the real *driving function*. The Löwner equation establishes an equivalence between the curve  $\gamma(s)$  and its driving function  $\xi(s)$ . Different driving functions produce different curves. In the case of random curves  $\gamma(s)$ , Eq. (7) is called stochastic Löwner evolution (SLE), and the driving  $\xi(s)$  is a random real variable. It has been demonstrated that the statistics of random curves are conformal invariant if and only if the driving is a Brownian walk, i.e., a random function with independent increments and with  $\langle (\xi(s) - \xi(0))^2 \rangle = \kappa s$ . Here  $\kappa$  is the diffusion coefficient which classifies the universality class of cluster boundaries in critical phenomena in two dimensions [32,34,35]. One of the predictions for SLE curves is their fractal dimension, which is known to be  $D = 1 + \kappa/8$  (for  $\kappa < 8$ ). In the case of critical percolation, for which  $\kappa = 6$ , the prediction is  $D = 7/4$ , which has been indeed measured in the vorticity cluster of 2D turbulence [10].

We have therefore extracted the zero-vorticity line from the fields of weakly compressible turbulence. The extraction is performed by means of an algorithm which follows the frontier of a cluster of vorticity by always keeping the positive region on the right of the path. At variance with “true” SLE curves, in our numerical simulation, scale (and conformal) invariance can be expected in the range of scales of the inverse cascade only. Therefore, for numerical convenience, we have coarse grained the vorticity fields produced by the simulation by halving the resolution to a  $4096 \times 4096$  grid. One example of a vorticity isoline obtained from this procedure is shown in

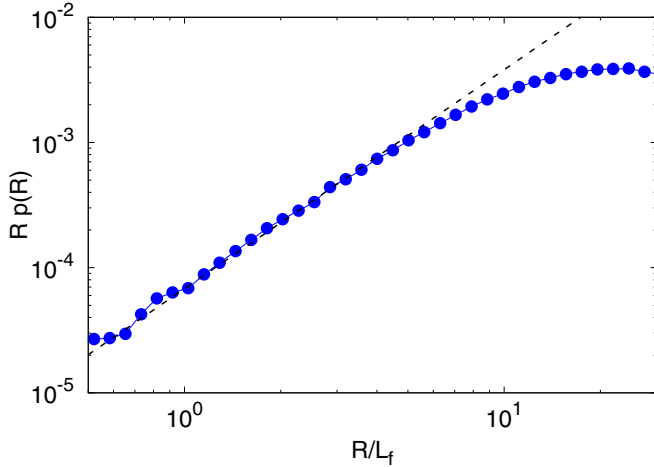


FIG. 6. Probability density function of distances  $R$  between two points belonging to the the same zero-vorticity line (blue circles). The black dashed line represents the theoretical prediction  $Rp(R) \sim R^{7/4}$ .

Fig. 4 (right panel). The total number of isolines obtained is  $N = 1144$ .

We have computed the correlation dimension  $D_2$  of the zero-vorticity isolines by computing the probability density function (PDF)  $p(R)$  of finding two points belonging to the same isoline at distance  $R$ . For a fractal set, the probability scales as  $p(R) \propto R^{D_2-1}$ . As shown in Fig. 6, the PDF  $p(R)$  displays a scaling exponent in agreement with the prediction for the SLE curves with  $\kappa = 6$ , i.e.,  $D_2 = 7/4$  in the range of scales  $1 \lesssim R/L_f \lesssim 7$ , which corresponds to the the inverse cascade.

Assuming that the ensemble of zero-vorticity isolines is statistically equivalent to SLE curves, we have derived the associated ensemble of driving functions  $\xi(s)$ . The algorithm which computes the driving for a generic curve is based on the solution of the Eq. (7) in the case of an infinitesimal line segment starting from the origin  $(0, 0)$  and ending in  $(\xi, 2\sqrt{ds})$ :  $g_{ds}(z) = \xi + \sqrt{(z - \xi)^2 + 4ds}$ . By approximating the generic curve  $\gamma(s)$  with piecewise line segments, one obtains the associated driving function  $\xi(s)$  (see Ref. [10] for further details). Averaging over the ensemble of  $N = 1144$  driving functions obtained, we have computed the variance  $\sigma_\xi^2 = \langle [\xi(s) - \langle \xi(s) \rangle]^2 \rangle$ . In the range  $1 \lesssim s/(2L_f)^2 \lesssim 7$ , we find that the variance grows linearly as  $\sigma_\xi^2 = \kappa s$  (see Fig. 7). The driving  $\xi(s)$  is therefore a diffusive process with  $\kappa \approx (5.7 \pm 0.2)$ , which is close (within the statistical uncertainty) to the expected value of  $\kappa = 6$ . Moreover, the PDF of the standardized driving  $[\xi(s) - \langle \xi(s) \rangle]/(\kappa s)^{1/2}$  collapses onto a standard Gaussian distribution function for values of  $s$  in the scaling range (see Fig. 8). These findings support the conjecture that the driving function is a genuine Brownian motion  $\xi_s = \sqrt{\kappa} B_s$ , and that the vorticity isolines are SLE curves belonging to the same class of universality of percolation corresponding to  $\kappa = 6$ .

The fact that the vorticity field of 2D compressible turbulence produces conformal invariant isoline in the same class of critical percolation deserve more discussion. It is well known that, in two dimensions, clusters produced by a random field

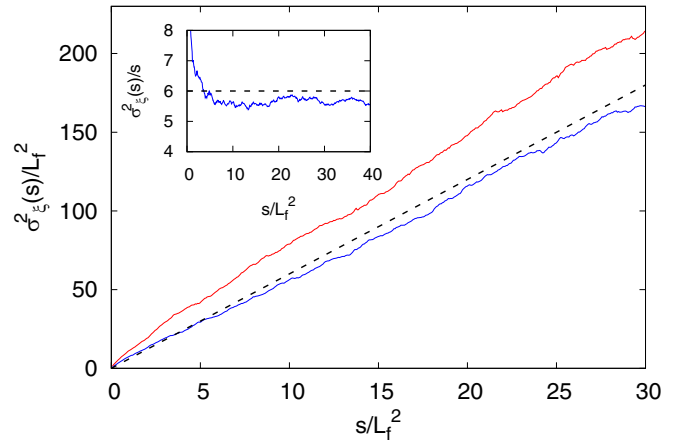


FIG. 7. Variance of driving function  $\sigma_\xi^2(s)$  as a function of the parametrization  $s$  for the vorticity field (blue solid line) and for the phase-randomized field (red solid line). The black dashed line represents the theoretical prediction  $\sigma_\xi^2(s) = \kappa s$  with  $\kappa = 6$ . In the inset we show the compensated value  $\sigma_\xi^2(s)/s$ .

with correlation function which decays as  $r^{-a}$  are in the same class of uncorrelated percolation (i.e., correlations are irrelevant) if  $a > 3/2$  [36]. Vorticity field in the inverse cascade is not short correlated since correlation function decays as  $r^{-4/3}$ , and therefore it is not expected to belong to the same class of uncorrelated percolation. Since  $4/3$  is close to  $3/2$  it is interesting to check if SLE analysis is able to discriminate between the turbulent vorticity field and a random field with the same scaling properties.

To this aim, we have studied the traces produced by the same data set of vorticity fields after phase randomization of the Fourier modes. In this way we produce a random field which has the same statistical properties of the original vorticity field (i.e., the same spectrum and correlation function) without the spatial structure produced by the dynamics. The result of the SLE analysis is plotted in Fig. 7 and shows that the random field is not compatible with critical percolation.

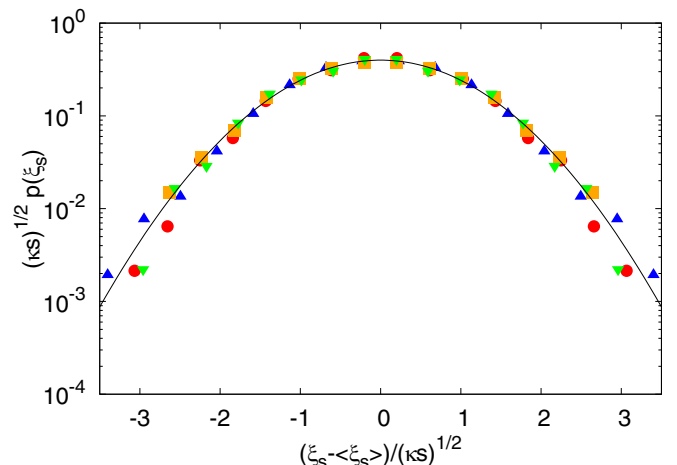


FIG. 8. PDF of the driving functions  $\xi_s$  at different values of  $s$ :  $s = 10L_f^2$  (blue upper triangles),  $s = 20L_f^2$  (red circles),  $s = 30L_f^2$  (orange squares),  $s = 40L_f^2$  (green lower triangles).

## V. CONCLUSIONS

In this work we have studied the conformal invariance of weakly compressible 2D turbulence. We have shown that the isolines of vorticity clusters are compatible with SLE curves in the universality class of critical percolation, as in the case of incompressible 2D turbulence. Our results therefore extend those obtained in other 2D turbulent systems (Navier-Stokes, surface quasigeostrophic, Charney-Hasegawa-Mima) to the realm of (weakly) compressible turbulence.

One question which naturally arises from our results is whether the conformal invariance property would survive in higher compressible regimes characterized by larger Mach numbers. While this is in principle interesting, we remark that, by increasing the Mach number, a different phenomenology emerges at large scales: When velocity fluctuations reach the speed of sound, kinetic energy produces shock waves which arrest the inverse cascade and provide a new mechanism

of energy dissipation [14]. This “flux loop” introduces a characteristic scale in the process which breaks the scaling invariance of the cascade. Conformal (and scaling) invariance could still survive in the limited range of scales between energy injection and shock wave production, and its study would be an interesting problem for future investigation.

## ACKNOWLEDGMENTS

G.B. and S.M. acknowledge financial support by the Departments of Excellence grant (MIUR). A.K. acknowledges support by the Binational Science Foundation under Grant No. 2018118. This work used the Extreme Science and Engineering Discovery Environment (XSEDE), including the *Comet* and *Data Oasis* systems at the San Diego Supercomputer Center, through allocation TG-MCA07S014 and Director’s Discretionary allocation DDP189.

- 
- [1] R. H. Kraichnan, Inertial ranges in two-dimensional turbulence, *Phys. Fluids* **10**, 1417 (1967).
  - [2] J. R. Herring and J. C. McWilliams, Comparison of direct numerical simulation of two-dimensional turbulence with two-point closure: The effects of intermittency, *J. Fluid Mech.* **153**, 229 (1985).
  - [3] M. E. Maltrud and G. K. Vallis, Energy spectra and coherent structures in forced two-dimensional and beta-plane turbulence, *J. Fluid Mech.* **228**, 321 (1991).
  - [4] L. M. Smith and V. Yakhot, Bose Condensation and Small-Scale Structure Generation in a Random Force Driven 2D Turbulence, *Phys. Rev. Lett.* **71**, 352 (1993).
  - [5] G. Boffetta, A. Celani, and M. Vergassola, Inverse energy cascade in two-dimensional turbulence: Deviations from Gaussian behavior, *Phys. Rev. E* **61**, 29(R) (2000).
  - [6] Z. Xiao, M. Wan, S. Chen, and G. L. Eyink, Physical mechanism of the inverse energy cascade of two-dimensional turbulence: A numerical investigation, *J. Fluid Mech.* **619**, 1 (2009).
  - [7] J. Paret and P. Tabeling, Experimental Observation of the Two-Dimensional Inverse Energy Cascade, *Phys. Rev. Lett.* **79**, 4162 (1997).
  - [8] M. Rivera, P. Vorobieff, and R. E. Ecke, Turbulence in Flowing Soap Films: Velocity, Vorticity, and Thickness Fields, *Phys. Rev. Lett.* **81**, 1417 (1998).
  - [9] S. Chen, R. E. Ecke, G. L. Eyink, M. Rivera, M. Wan, and Z. Xiao, Physical Mechanism of the Two-Dimensional Inverse Energy Cascade, *Phys. Rev. Lett.* **96**, 084502 (2006).
  - [10] D. Bernard, G. Boffetta, A. Celani, and G. Falkovich, Conformal invariance in two-dimensional turbulence, *Nat. Phys.* **2**, 124 (2006).
  - [11] D. Bernard, G. Boffetta, A. Celani, and G. Falkovich, Inverse Turbulent Cascades and Conformally Invariant Curves, *Phys. Rev. Lett.* **98**, 024501 (2007).
  - [12] G. Falkovich and S. Musacchio, Conformal invariance in inverse turbulent cascades, [arXiv:1012.3868](https://arxiv.org/abs/1012.3868).
  - [13] Stefanus, J. Larkin, and W. I. Goldburg, Search for conformal invariance in compressible two-dimensional turbulence, *Phys. Fluids* **23**, 105101 (2011).
  - [14] G. Falkovich and A. G. Kritsuk, How vortices and shocks provide for a flux loop in two-dimensional compressible turbulence, *Phys. Rev. Fluids* **2**, 092603 (2017).
  - [15] J.-M. Chomaz, The dynamics of a viscous soap film with soluble surfactant, *J. Fluid Mech.* **442**, 387 (2001).
  - [16] M. Chertkov, C. Connaughton, I. Kolokolov, and V. Lebedev, Dynamics of Energy Condensation in Two-Dimensional Turbulence, *Phys. Rev. Lett.* **99**, 084501 (2007).
  - [17] K. A. Naugol’nykh, Nonlinear sound waves upon collapse of a vortex dipole, *Acoust. Phys.* **60**, 424 (2014).
  - [18] H. Xia, M. Shats, and G. Falkovich, Spectrally condensed turbulence in thin layers, *Phys. Fluids* **21**, 125101 (2009).
  - [19] S. Musacchio and G. Boffetta, Condensate in quasi-two-dimensional turbulence, *Phys. Rev. Fluids* **4**, 022602 (2019).
  - [20] M. J. Lighthill, The effect of compressibility on turbulence, in *Gas Dynamics of Cosmic Clouds*, edited by H. G. van de Hulst and J. M. Burgers (North Holland, Amsterdam, 1955), pp. 121–130.
  - [21] J. W. Miles, On the reflection of sound at an interface of relative motion, *Acoust. Soc. Amer. J.* **29**, 226 (1957).
  - [22] M. Artola and A. J. Majda, Nonlinear development of instabilities in supersonic vortex sheets. II—Resonant interaction among kink modes, *SIAM J. Appl. Math.* **49**, 1310 (1989).
  - [23] G. Boffetta, F. De Lillo, A. Mazzino, and S. Musacchio, A flux loop mechanism in two-dimensional stratified turbulence, *Europhys. Lett.* **95**, 34001 (2011).
  - [24] I. V. Sytine, D. H. Porter, P. R. Woodward, S. W. Hodson, and K.-H. Winkler, Convergence tests for the piecewise parabolic method and Navier–Stokes solutions for homogeneous compressible turbulence, *J. Comput. Phys.* **158**, 225 (2000).
  - [25] P. Colella and P. R. Woodward, The piecewise parabolic method (PPM) for gas-dynamical simulations, *J. Comput. Phys.* **54**, 174 (1984).
  - [26] G. L. Bryan, M. L. Norman, B. W. O’Shea, T. Abel, J. H. Wise, M. J. Turk, D. R. Reynolds, D. C. Collins, P. Wang, S. W. Skillman *et al.*, Enzo: An adaptive mesh refinement code for astrophysics, *Astrophys. J. Supp. Series* **211**, 19 (2014).
  - [27] A. G. Kritsuk, Energy transfer and spectra in simulations of two-dimensional compressible turbulence, in *Turbulence*

- Cascades II*, edited by M. Gorokhovski and F. S. Godeferd, ERCOFTAC Series Vol. 26 (Springer, Cham, Switzerland, 2019), pp. 61–70.
- [28] D. Bernard, Three-point velocity correlation functions in two-dimensional forced turbulence, *Phys. Rev. E* **60**, 6184 (1999).
- [29] E. Lindborg, Can the atmospheric kinetic energy spectrum be explained by two-dimensional turbulence? *J. Fluid Mech.* **388**, 259 (1999).
- [30] D. Stauffer and A. Aharony, *Introduction to Percolation Theory* (Taylor & Francis, London, UK, 2010).
- [31] O. Schramm, Scaling limits of loop-erased random walks and uniform spanning trees, *Isr. J. Math.* **118**, 221 (2000).
- [32] J. Cardy, SLE for theoretical physicists, *Ann. Phys.* **318**, 81 (2005).
- [33] K. Löwner, Untersuchungen über schlichte konforme Abbildungen des Einheitskreises. I, *Mat. Ann.* **89**, 103 (1923).
- [34] M. Bauer and D. Bernard, Conformal field theories of stochastic Loewner evolutions, *Comm. Math. Phys.* **239**, 493 (2003).
- [35] I. A. Gruzberg and L. P. Kadanoff, The Loewner equation: Maps and shapes, *J. Stat. Phys.* **114**, 1183 (2004).
- [36] A. Weinrib, Long-range correlated percolation, *Phys. Rev. B* **29**, 387 (1984).